Rapid Communications

Anharmonic lattice relaxation during nonradiative carrier capture

Sunghyun Kim,[1,*] Samantha N. Hood,[1] and Aron Walsh[1,2,†]
[1]*Department of Materials, Imperial College London, SW7 2AZ, United Kingdom*
[2]*Department of Materials Science and Engineering, Yonsei University, Seoul 03722, Korea*

(Received 2 April 2019; revised manuscript received 21 June 2019; published 22 July 2019)

Lattice vibrations of point defects are essential for understanding nonradiative electron and hole capture in semiconductors as they govern properties including persistent photoconductivity and the Shockley-Read-Hall recombination rate. Although the harmonic approximation is sufficient to describe a defect with small lattice relaxation, for cases of large lattice relaxation it is likely to break down. We describe a first-principles procedure to account for anharmonic carrier capture and apply it to the important case of the *DX* center in GaAs. This is a system where the harmonic approximation grossly fails. Our treatment of the anharmonic Morse-like potentials accurately describes the observed electron capture barrier, predicting the absence of quantum tunneling at low temperature, and a high hole capture rate that is independent of temperature. The model also explains the origin of the composition-invariant electron emission barrier. These results highlight an important shortcoming of the standard approach for describing point defect ionization that is accompanied by large lattice relaxation, where charge transfer occurs far from the equilibrium configuration.

DOI: 10.1103/PhysRevB.100.041202

Introduction. Following the pioneering work of Landau and Zener [1], nonradiative charge transfer has been studied extensively in molecules and biological systems [2], as well as in condensed matter [3,4]. In the Landau-Zener formula, the probability of charge transfer is proportional to the square of the coupling of initial and final states and inversely proportional to the rate of change in their energy spacing. For point defects in crystalline solids, with quantized vibrations [3–8], the carrier capture coefficient C can be expressed using the electron-phonon coupling $\langle\psi_i|\partial H/\partial Q|\psi_f\rangle$ and the overlap of vibrational wave functions $\langle\xi_{im}|\Delta Q|\xi_{fn}\rangle$, which is given by

$$C = \frac{2\pi}{\hbar}|\langle\psi_t|\partial H/\partial Q|\psi_c\rangle|^2 \times \sum_{m,n} w_m|\langle\xi_{tn}|\Delta Q|\xi_{cm}\rangle|^2\delta(E_{cm}-E_{tn}), \quad (1)$$

where ψ and ξ are electronic and vibrational wave functions, respectively, and the subscripts c and t specify the free carrier and trap states. E_{cm} and E_{tn} denote the energy of the carrier and trap states, respectively, where m and n are the indices for vibrational eigenstates. Here, we use the effective configuration coordinate Q.

In this formalism, the temperature dependence is determined by the thermal occupation number w_m of the initial vibrational state. Early theories provided a good understanding of carrier capture rates that follow Arrhenius behavior at high temperature and are limited by quantum mechanical tunneling at low temperature. However, it is impossible to access the detailed parameters experimentally, including electron-phonon coupling matrix elements and overlap integrals of vibrational wave functions. Instead, the weighted average of the capture rate is measured.

Modern simulation approaches have been based on density functional theory (DFT) that avoids the need for empirical parameters. Shi and Wang [6] proposed an adiabatic formalism to calculate the capture rate using DFT, taking into account the full set of phonon modes for a given defect. Later, a method adopting a one-dimensional (1D) configuration coordinate and static coupling theory was proposed by Alkauskas *et al.* [7]. The two methods have been compared, and the validity of the 1D configuration coordinate has been confirmed [9–11]. The adiabatic approximation generally underestimates the capture rate compared to measurements and static coupling theory [9–11], while Barmparis *et al.* [8] showed that a nonequilibrium adiabatic term can be larger than the nonadiabatic term. However, as they both adopt the harmonic approximation for the potential energy surface (PES) of defects, the role of anharmonicity in nonradiative carrier capture has not been well characterized. The vibrations of a defect may differ significantly from harmonic behavior when its atomic configuration is far from the equilibrium structure, as has been suggested in earlier work [4,5,12].

Carrier capture that occurs far from an equilibrium configuration has been understood based on a large-lattice-relaxation (LLR) model developed by Lang and Logan [13]. The LLR model successfully explained persistent photoconductivity (PPC) in $Al_xGa_{1-x}As$ ($x > 0.22$) and GaAs under hydrostatic pressure with the lack of quantum tunneling at low temperature (<77 K) and a large Stokes shift of ca. 1 eV. The model adopts the harmonic approximation with empirical parametrization, although the authors mentioned that anharmonic terms may be important.

One of the most intensively studied LLR defects is the *DX* center in $Al_xGa_{1-x}As$, owing not only to its anomalous physical properties but also its technological importance. The

*sunghyun.kim@imperial.ac.uk
†a.walsh@imperial.ac.uk

isolated substitutional Si atom (Si_{Ga}) was proposed as an atomic model of the *DX* center by Chadi and Chang [14,15], and successfully explained experimental observations. However, a detailed microscopic understanding has not been fully explored. Unusually, the electron emission barrier is invariant with respect to the variation in the composition of $Al_xGa_{1-x}As$ and hence the donor binding energy [16,17]. With only circumstantial evidence, it has been assumed that the transition from the conduction band minimum at the Γ point to the *DX* center is forbidden, and a hypothetical intermediate state, presumably related to the *L* valley of the conduction band, plays an important role [16–18].

In this Rapid Communication, we report a first-principles anharmonic approach to describe nonradiative electron and hole capture in semiconductors. We apply it to investigate carrier trapping by the *DX* center, Si_{Ga}, in GaAs under hydrostatic pressure. During the atomic transformation accompanying carrier capture, the bond-breaking relaxation of Si_{Ga} results in a Morse-like PES. Here, the harmonic approximation significantly overestimates the electron and hole capture barriers and fails to even qualitatively describe the physical behavior of the system.

Our procedure is implemented in the open-source CARRIERCAPTURE.JL package [19]. We followed static coupling theory as implemented by Alkauskas *et al.* [7], but removed the restriction of harmonic vibrations. Instead we calculate the vibrational wave functions ξ and matrix elements $\langle \xi_{in} | \Delta Q | \xi_{cm} \rangle$ from solutions of the 1D Schrödinger equation for the anharmonic PES using a finite-difference method. Further details of the methodology can be found in the literature [7]. The total energy of pristine and defective crystals was calculated from DFT [20,21] using the projector augmented-wave (PAW) method [22] and the hybrid exchange-correlation functional of Heyd-Scuseria-Ernzerhof (HSE06) [23], as implemented in VASP [24]. We used a value of screened exact exchange ($\alpha = 0.28$) that reproduces the experimental band gap of GaAs. The wave functions were expanded in plane waves up to an energy cutoff of 400 eV. The all-electron wave functions were derived from the pseudowave functions and atom-centered partial waves in the PAW method, and the overlap integrals were performed in real space using PAWPYSEED [25] to calculate the electron-phonon coupling outlined by Alkauskas *et al.* [7]. A Monkhorst-Pack *k* mesh [26] with a grid spacing less than $2\pi \times 0.03$ Å^{-1} was used for Brillouin zone integration. The atomic coordinates were optimized until the residual forces were less than 0.01 eV/Å. The lattice vectors were relaxed until residual stress was below 0.5 kbar under an external pressure of 28 kbar, which is a regime where the *DX* center is stable. For defect formation, a $3 \times 3 \times 3$ supercell expansion (216 atoms) of the conventional cell was employed with Γ-point sampling to avoid spurious dispersion of the Kohn-Sham eigenstates for the defect.

Anharmonicity of the DX center. Si_{Ga} is a shallow donor in GaAs. The defect with T_d symmetry is referred to as the *d* configuration [Fig. 1(a)]. In both GaAs under hydrostatic pressure and the $Al_xGa_{1-x}As$ ($x > 0.22$) alloy, the band gap is widened and a shallow-to-deep transition occurs. A deep donor, the so-called *DX* configuration with C_{3v} symmetry, becomes stable [Fig. 1(b)]. In the *DX* configuration, the

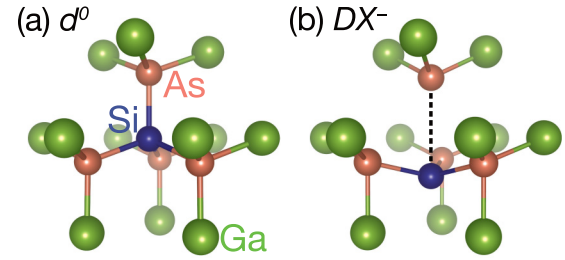

FIG. 1. Atomic structures of Si_{Ga} in (a) the neutral *d* and (b) negatively charged *DX* configurations. Only second-nearest-neighbor atoms are shown, for clarity. For the *DX* configuration, the broken Si-As bond is represented by a dashed line.

Si-As bond is broken and the Si atom exhibits a large lattice relaxation toward the antibonding site. We find that the neutral *d* configuration produces a shallow level with a delocalized Kohn-Sham eigenstate, while the negatively charged *DX* produces a deep eigenstate localized around a Si-As antibonding orbital. This doubly occupied antibonding level stabilizes the *DX* configuration.

To begin, we mapped the PES of the Si_{Ga} defect over a configuration coordinate *Q* that represents the degree of collective atomic deformation (Fig. 2). *Q* is defined by

$$Q^2 = \sum_{\alpha} M_{\alpha} \Delta \mathbf{R}_{\alpha}^2, \tag{2}$$

where M_α and $\Delta \mathbf{R}_\alpha$ are the atomic mass and the displacement vector from the equilibrium position of atom α, respectively.

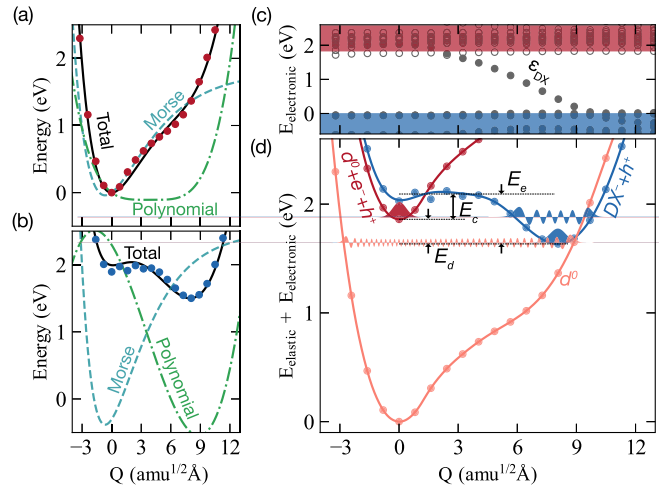

FIG. 2. Potential energy surfaces of (a) d^0 and (b) DX^- configurations of Si_{Ga} in GaAs. The black solid line shows the best fit to the DFT data represented by solid circles. The best fit curves are composed of the Morse function (blue dashed line) and polynomial functions (green dashed-dotted line). (c) Evolution of Kohn-Sham eigenstates of the supercell containing DX^- with respect to the deformation of the geometry along *Q*. Solid and open circles represent occupied and unoccupied states, respectively. (d) Configuration coordinate diagram for electron and hole capture. The solid circle and lines depict the DFT results and the quadratic spline fit to the DFT data, respectively. The vibrational wave functions for the ground state of initial PES and the corresponding final state are shown.

This is an effective 1D coordinate that replaces the multidimensional phonon modes. It has been shown that this choice of 1D configuration coordinate is a good approximation to the multidimensional approach and successfully reproduces experimental line shapes for the defects with large lattice relaxations [27].

The PESs of d and DX are well described by a combination of two forms: a Morse potential and a polynomial potential up to fourth order that describe the Si-As bond breaking, and additional bond stretching and bond bending around the defect, respectively. For neutral d^0, the stretching of the Si-As bond increases the potential energy significantly over a short range, but after the bond breaking ($Q > 4$ amu$^{1/2}$ Å), the energy increases moderately due to the bending of other bonds [Fig. 2(a)]. Further distortion results in a substantial energy penalty.

For the charged DX^-, the polynomial potential shows a minimum around the DX configuration (8.8 amu$^{1/2}$ Å), while the minimum of the Morse potential is near the d configuration (-0.7 amu$^{1/2}$ Å). Thus, the Morse potential describes the attractive force between Si and As compensating the restoring force due to the perturbation of other bonds [Fig. 1(b)]. This competition results in the soft anharmonic PES of DX^- near the d configuration. Further distortion results in a strong Pauli repulsion which takes an exponential form. Despite their simplicity, the combination of Morse and polynomial potentials adequately describes the DFT energy surface and produces a physical dissociation energy of 2–3 eV for the Morse component.

Note that the anharmonicity of the potentials is not due to the adiabatic anticrossing discussed in Ref. [9]. Here, it is because of the failure of Hooke's law upon the large lattice relaxation.

The evolution of the electronic eigenstate during the lattice relaxation from DX^- to d^0 is shown in Fig. 2(c). As the Si and As atoms approach, the antibonding level rises toward the conduction band edge; at $Q = 2.4$ amu$^{1/2}$ Å they cross. It is challenging to describe a diabatic level crossing within the framework of the DFT/Born-Oppenheimer approximation due to a variational collapse. Our practical solution is to employ a Δ self-consistent field approach and constrain the occupation of the defect level. This approach recovers the diabatic process, but results in some noise near the crossing point [Fig. 2(b)] as the adiabatic basis is strongly coupled. The development and application of more sophisticated excited-state techniques such as time-dependent DFT is a worthwhile line of research.

The full configuration coordinate diagram describing electron capture [Fig. 2(d)] is obtained by aligning the PES of d^0 and DX^- using the donor binding energy (E_d) of the DX center, which varies from 0 to 0.23 eV depending on AlAs mole fraction x in $Al_xGa_{1-x}As$ [17] and the hydrostatic pressure [16,28,29]. While the decomposition of the PES into intuitive functions is useful for a qualitative analysis, we use quartic splines for the best fit to the DFT energy surface [Fig. 2(d)].

One anomaly of the DX center is that the activation energy for electron emission E_e is nearly invariant with respect to the AlAs mole fraction x and hence the donor binding energy as shown in Fig. 3. This weak variation in E_e cannot be explained by configuration coordinates within the harmonic approximation. We have calculated the emission barrier with various donor binding energies (Fig. 3). The AlAs mole fraction x is estimated based on the donor binding energy measured by deep level transient spectroscopy (DLTS). Due to the plateau in the potential of DX^- around $Q = 3$ amu$^{1/2}$ Å, the activation energy for electron emission E_e is fixed to 0.45 eV, which is the height of the plateau above the vibrational ground state regardless of the donor binding energy. Thus, it is the anharmonicity of DX^- that results in the constant E_e. The intermediate state that has been proposed previously [16–18] is not required. Furthermore, the calculated energy barrier for electron capture also agrees well with experiments [17]. The donor binding energy measured by Hall experiments (Fig. 3) results in a slightly higher capture energy, as they predict shallower levels [30].

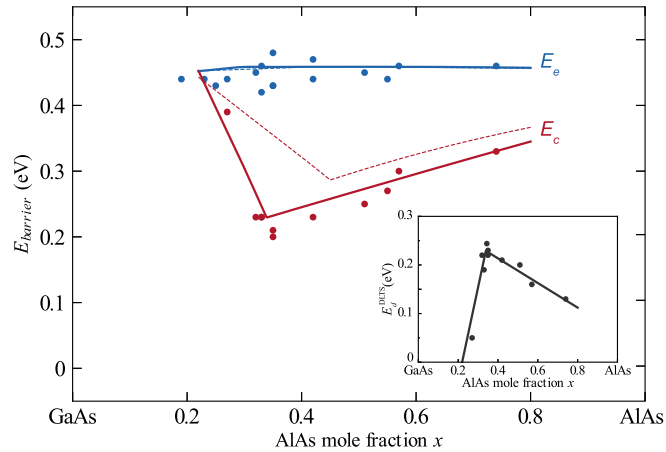

FIG. 3. Energy barriers for electron emission (blue line) and electron capture (red line) in $Al_xGa_{1-x}As$. The experimental data (solid circles) are taken from Ref. [17]. The calculated energy barriers are presented as a function of the molar fraction x estimated using the empirical donor binding energy (E_d) measured by DLTS [17] (solid lines) and Hall experiments [30] (dashed lines). The inset shows the donor binding energy E_d^{DLTS} (solid line) obtained from the best fit to the DLTS data (solid circles).

Rate of carrier capture. The anharmonic PES significantly lowers the electron capture barrier as compared to predictions within the harmonic approximation. The calculated electron capture barriers are 0.2–0.4 eV, depending on the donor binding energy, which agrees well with experiments [17]. The harmonic approximation predicts much higher barriers of 1.5–1.6 eV.

Next, we calculate the electron capture cross section,

$$\sigma_n = C_n/\langle v_{\mathrm{th}}\rangle, \tag{3}$$

where the thermal velocity $\langle v_{\mathrm{th}}\rangle = \sqrt{3k_BT/m^*}$ is calculated using the effective masses m^* of carriers taken from Ref. [31]. Here, we use the atomic structure of DX^- for the unperturbed state to calculate C_n. This is because DX^- introduces a single-particle Kohn-Sham eigenstate well isolated in the band gap, making it essential for static coupling theory [7], while the eigenvalue of d^0 is located above the conduction band minimum [see Fig. 2(c)].

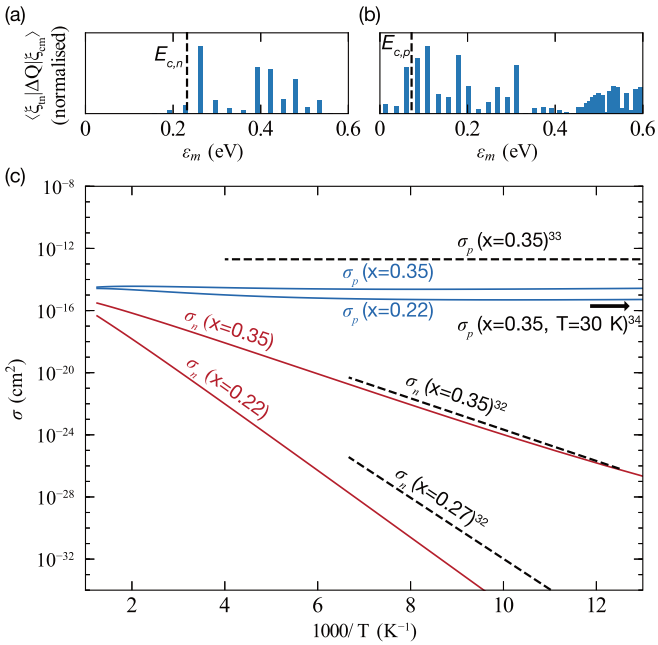

FIG. 4. Overlap of vibrational wave functions with energy ϵ_m for (a) electron capture and (b) hole capture of the *DX* center with a donor binding energy of 0.2 eV. $E_{c,n}$ and $E_{c,p}$ represent the electron and hole barrier heights, respectively. (c) Blue and red solid lines represent calculated electron and hole capture cross sections of the *DX* center. The measured cross sections (dashed lines and arrows) are taken from Ref. [32] for electron capture and Refs. [33,34] for hole capture.

The high-temperature behavior of carrier capture is often governed by a classical energy barrier while, at low temperature, tunneling is dominant. However, for the *DX* center, the overlap of vibrational wave functions is negligible below the energy barrier, as shown in Fig. 4(a), due to the large lattice relaxation and the long plateau in energy of DX^- [Fig. 2(d)]. Thus, tunneling is suppressed and its effect is negligible. The calculated electron capture cross section decreases exponentially, even at a low temperature of around 77 K [Fig. 4(c)], which explains the experimental observations [32].

In contrast, hole capture occurs with a large overlap of vibrational wave functions even below the small energy barrier, as shown in Fig. 4(b). This explains the weak temperature dependence in the hole capture cross sections. Moreover, the parallel PESs ($Q > 9$ amu$^{1/2}$ Å) of d^0 and DX^- produce large overlap populations above the crossing point [Fig. 4(b)]. Here, the harmonic approximation predicts much smaller cross sections due to the high hole capture barrier of 1 eV. On the other hand, the Morse component alone does not cross the potential energy surface of DX^-, which predicts that the vibrational wave function is unbounded, and only radiative recombination is allowed. The restoring force on the Si atom provided by the remaining three Si-As bonds ensures bound states with high energy and a large hole capture cross section. After the hole capture, the excess energy is dissipated by emitting multiple phonons, which is mainly attributed to the Morse potential, forming the Si-As bond [Fig. 2(a)].

Finally, we stress that the 1D configuration coordinate is an approximation to multidimensional energy surfaces [6,8,9]. Thus, the calculated energy barriers and capture cross sections must be considered as the upper bounds and lower bounds of the true values, respectively. However, we find good agreement between the calculations and the experiments [see Figs. 3 and 4(c)], which we attribute to the simple atomic motion of the *DX* center during the bond-break relaxation.

In summary, we have shown that anharmonicity can play an important role in the nonradiative carrier capture process mediated by defects in semiconductors. Due to the bond-breaking relaxation by the *DX* center in GaAs, we find a large lattice relaxation with a Morse-like potential. The abnormal insensitivity of the activation energy for electron emission to the AlAs mole fraction can be explained by the anharmonicity of the potential. The calculated carrier capture cross sections of *DX* center agree well with experiments and differ significantly from those predicted from the harmonic approximation. The anharmonic potential energy surfaces of the *DX* center enhance the hole capture process and make it weakly dependent on temperature. Thus we conclude that the harmonic approximation is insufficient when the charge transition occurs far from the equilibrium configuration, even if the full phonon spectrum is considered. One should consider the whole shape of the potential energy surface including the anharmonicity of atomic vibrations.

Our computer codes and data are available at an open-access repository [19], allowing other researchers to reproduce our results.

Acknowledgments. We thank Lucy D. Whalley and Ji-Sang Park for valuable discussions, and Audrius Alkauskas for helpful comments on our manuscript. This work was supported by the EU Horizon2020 Framework (STARCELL, Grant No. 720907). Additional funds were received from the Creative Materials Discovery Program through the National Research Foundation of Korea (NRF) funded by Ministry of Science and ICT (2018M3D1A1058536). Via our membership of the UK's HEC Materials Chemistry Consortium, which is funded by EPSRC (EP/L000202), this work used the ARCHER U.K. National Supercomputing Service [35].

[1] C. Zener, Proc. R. Soc. London, Ser. A **137**, 696 (1932).
[2] R. A. Marcus and N. Sutin, Biochim. Biophys. Acta **811**, 265 (1985).
[3] K. Huang, A. Rhys, and A. Rhys, Proc. R. Soc. London, Ser. A **204**, 406 (1950).
[4] C. H. Henry and D. V. Lang, Phys. Rev. B **15**, 989 (1977).
[5] A. M. Stoneham, *Theory of Defects in Solids* (Oxford University Press, Cambridge, UK, 1975).
[6] L. Shi and L.-W. Wang, Phys. Rev. Lett. **109**, 245501 (2012).
[7] A. Alkauskas, Q. Yan, and C. G. Van de Walle, Phys. Rev. B **90**, 075202 (2014).

[8] G. D. Barmparis, Y. S. Puzyrev, X. G. Zhang, and S. T. Pantelides, Phys. Rev. B **92**, 214111 (2015).
[9] L. Shi, K. Xu, and L.-W. Wang, Phys. Rev. B **91**, 205315 (2015).
[10] D. Wickramaratne, J.-X. Shen, A. Alkauskas, and C. G. Van de Walle, Phys. Rev. B **97**, 077301 (2018).
[11] L. Shi, K. Xu, and L.-W. Wang, Phys. Rev. B **97**, 077302 (2018).
[12] T. Markvart, J. Phys. C: Solid State Phys. **14**, L435 (1981).
[13] D. V. Lang and R. A. Logan, Phys. Rev. Lett. **39**, 635 (1977).
[14] D. J. Chadi and K. J. Chang, Phys. Rev. Lett. **61**, 873 (1988).
[15] D. J. Chadi and K. J. Chang, Phys. Rev. B **39**, 10063 (1989).
[16] E. Calleja, A. Gomez, and E. Muñoz, Appl. Phys. Lett. **52**, 383 (1988).
[17] P. M. Mooney, N. S. Caswell, and S. L. Wright, J. Appl. Phys. **62**, 4786 (1987).
[18] A. K. Saxena, Solid-State Electron. **25**, 127 (1982).
[19] S. Kim, S. N. Hood, and A. Walsh, CARRIERCAPTURE, http://dx.doi.org/10.5281/zenodo.2621017 (2019).
[20] P. Hohenberg and W. Kohn, Phys. Rev. **136**, B864 (1964).
[21] W. Kohn and L. J. Sham, Phys. Rev. **140**, A1133 (1965).
[22] P. E. Blöchl, Phys. Rev. B **50**, 17953 (1994).
[23] J. Heyd, G. E. Scuseria, and M. Ernzerhof, J. Chem. Phys. **118**, 8207 (2003).
[24] G. Kresse and D. Joubert, Phys. Rev. B **59**, 1758 (1999).
[25] K. Bystrom, D. Broberg, S. Dwaraknath, K. A. Persson, and M. Asta, arXiv:1904.11572.
[26] H. J. Monkhorst and J. D. Pack, Phys. Rev. B **13**, 5188 (1976).
[27] A. Alkauskas, J. L. Lyons, D. Steiauf, and C. G. Van de Walle, Phys. Rev. Lett. **109**, 267401 (2012).
[28] T. Fujisawa, J. Krištofik, J. Yoshino, and H. Kukimoto, Jpn. J. Appl. Phys **27**, L2373 (1988).
[29] T. Fujisawa, J. Cryst. Growth **98**, 243 (1989).
[30] N. Chand, T. Henderson, J. Klem, W. T. Masselink, R. Fischer, Y.-C. Chang, and H. Morkoĉ, Phys. Rev. B **30**, 4481 (1984).
[31] M. Levinshtein, S. Rumyantsev, and M. Shur, *Handbook Series on Semiconductor Parameters* (World Scientific, Singapore, 1999), Vol. 2.
[32] P. M. Mooney, J. Appl. Phys. **67**, R1 (1990).
[33] G. Brunthaler, K. Ploog, and W. Jantsch, Phys. Rev. Lett. **63**, 2276 (1989).
[34] L. Dobaczewski, P. Kaczor, Z. R. Żytkiewicz, M. Missous, F. Saleemi, P. Dawson, and A. R. Peaker, J. Appl. Phys. **72**, 3198 (1992).
[35] http://www.archer.ac.uk